Eur. Phys. J. B **50**, 425–430 (2006)
DOI: 10.1140/epjb/e2006-00160-7

THE EUROPEAN PHYSICAL JOURNAL B

Magnetic properties, Mössbauer effect and first principle calculations study of laves phase $HfFe_2$

J. Belošević-Čavor[1,a], V. Koteski[1], N. Novaković[1], G. Concas[2], F. Congiu[2], and G. Spano[2]

[1] Institute of Nuclear Sciences Vinca, P.O. Box 522, 11001 Belgrade, Serbia and Montenegro
[2] Dipartimento di Fisica, Università di Cagliari and CNISM, S. P. Monserrato-Sestu km 0.700, Monserrato (CA), 09042, Italy

Received 30 November 2005 / Received in final form 13 February 2006
Published online 5 May 2006 –

Abstract. The magnetic properties and hyperfine interaction parameters for Laves phase $HfFe_2$ with C14 type structure are studied using SQUID magnetometer and Mössbauer measurement. The saturation magnetization, remanent magnetization, coercive field, magnetic moment per unit formula and the hyperfine magnetic field at Fe site are reported. In addition, a detailed theoretical study of the electronic structure and hyperfine magnetic fields of the two possible $HfFe_2$ structures, C15 and C14, is presented. Using the full-potential linearized augmented plane wave (FP-LAPW) method as implemented in the WIEN 97 package, the equilibrium volume, bulk moduli, magnetic moments and hyperfine magnetic fields for the two structures are calculated. The obtained results are compared with the measured data.

PACS. 71.15.Ap Basis sets – 71.20.Lp Intermetallic compounds – 71.20.Be Transition metals and alloys – 75.50.Bb Fe and its alloys

1 Introduction

The magnetic properties of Laves phase compounds of AB_2-type, where A is a transition metal and B is iron, have been extensively investigated in the past [1–6]. It is known since a long time that Laves phase intermetallic compounds with Fe-base, like $TMFe_2$ (TM = Zr, Hf, Ti, Sc) show more or less strong magnetovolume effects (Invar-like behaviour) in their thermal expansion, besides a rich spectrum of other magnetic anomalies [7].

$HfFe_2$ is a representative of this group of compounds that provides the possibility of observing hyperfine interactions at both sites: at Hf by TDPAC on the ^{181}Hf cascade and at Fe by Mössbauer spectroscopy in the ^{57}Fe nuclei. $HfFe_2$ has a C15 cubic structure of $MgCu_2$ type which exists in a narrow composition range around the stoichiometry. Additionally, it crystallizes in $MgZn_2$ (C14) hexagonal structure type.

The hyperfine interactions and magnetic properties of $HfFe_2$, in both of its crystallographic modifications, have been extensively investigated in the past. Ikeda [1] has shown that $HfFe_2$ is ferromagnetic in the hexagonal as well as in the cubic phase and measured two slightly different values for their saturation magnetization. Livi et al. [3] revealed that many of the difficulties encountered in the study of this compound can be understood as originating in an instability of the cubic phase, with formation of segregations of an hexagonal phase C14 structure, the amount and size of which depend on the preparation procedure of the sample [8]. Their study of the $HfFe_2$ predominantly cubic phase has revealed a population ratio of 3:1 for the magnetically inequivalent Fe sites, indicating that the easy direction of magnetization is along the $\langle 111 \rangle$ direction. Investigating the pseudo-binary system $Zr_xHf_{1-x}Fe$, Akselrod et al. [9] have come to the conclusion that for $x < 0.2$, the hexagonal phase appears in addition to the predominant cubic phase, whereas in the samples of pure $HfFe_2$ the C14 phase seems to prevail. Xia et al. [10] have recorded room temperature Mossbauer spectrum of the C14 $MgZn_2$ Laves structure, which displays two magnetic sub-spectra attributed to the two crystalographically inequivalent Fe atoms.

Despite the obvious interest in the magnetic properties and hyperfine interactions of this compound there are still some open questions, mainly regarding the electronic origin of the measured hyperfine fields.

Here we present Mossbauer and magnetization measurements of $HfFe_2$ with hexagonal C14 structure. In order to interpret the obtained results we have performed ab-initio calculations of the electronic structure and hyperfine magnetic fields (HMF). Since experimental data for the other structural modification of $HfFe_2$ exist in literature, we also present results of our theoretical calculations for the cubic C15 structure. In addition, we have determined a number of structural and electronic ground state properties for both structures.

[a] e-mail: cjeca@vin.bg.ac.yu

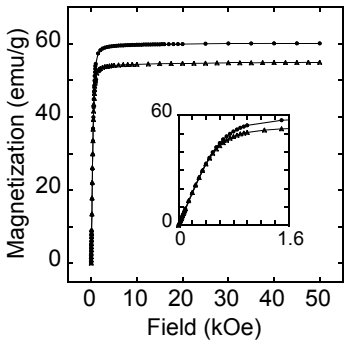

Fig. 1. First magnetization vs. applied magnetic field recorded at 5 K (dots) and 298 K (triangles) for the $HfFe_2$ sample. The inset shows the first magnetization in the region $0 \leq H \leq 1.6$ kOe. The line connects the experimental points.

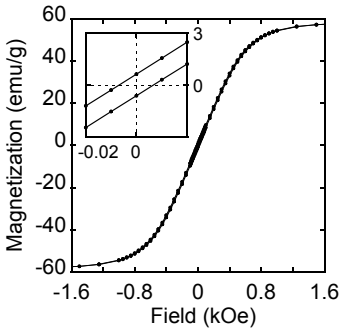

Fig. 2. Hysteresis loop (magnetization vs. applied magnetic field) recorded at 5 K for the $HfFe_2$ sample. The inset shows the loop in the region $H = \pm 0.02$ kOe. The line connects the experimental points.

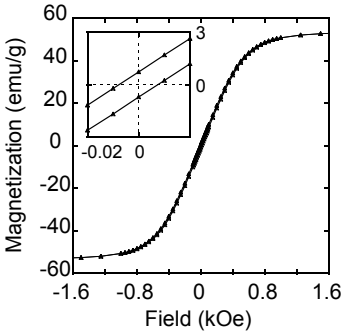

Fig. 3. Hysteresis loop (magnetization vs. applied magnetic field) recorded at 298 K for the $HfFe_2$ sample. The inset shows the loop in the region $H = \pm 0.02$ kOe. The line connects the experimental points.

2 Experimental details

The $HfFe_2$ sample was obtained in a radio-frequency induction furnace under pure argon atmosphere. The component materials were of high purity, 99.99% iron and 99.97% hafnium. All the peaks of the X-ray diffraction pattern can be indexed with the hexagonal C14 structure, but the presence of a small percent of C15 phase can not be ruled out. The magnetic properties of the sample have been investigated by Mössbauer spectroscopy and magnetization measurements using a superconducting quantum interference device (SQUID) magnetometer.

The magnetization measurements as a function of applied field were performed using a Quantum Design MPMS 5 XL 5 SQUID magnetometer, equipped with a superconducting magnet producing fields up to 50 kOe and calibrated using a Pd standard; the sensitivity for the magnetic moment is 10^{-8} emu. The first magnetization curves and hysteresis loops have been recorded at 5 K and 298 K; the mass of the sample was 12 mg.

The Mössbauer absorption spectrum was obtained in a standard transmission geometry, using a source of ^{57}Co in rhodium (37 MBq). A calibration was performed using a 25 μm thick natural α-iron foil; the isomer shift values are referred to α-iron. The measurement was carried out at room temperature on the powder sample contained in a plexiglas holder; the surface density of the absorber was 10 mg/cm^2. The spectrum has been examined by fitting the data by peaks with Lorentzian shape, using a least squares method.

3 Experimental results

Figure 1 presents the initial magnetization curve of $HfFe_2$, recorded at 5 K and 298 K. The hysteresis loop, recorded at 5 K is shown in Figure 2. The hysteresis loop is very narrow, with small values of the remanent magnetization and coercive field, as can be observed in more detail in the inset. The room temperature hysteresis loop is shown in Figure 3. There are only faint differences with respect to the low temperature loop, as it can be better observed in the inset, where the details of the loop in the region –20 Oe $< H <$ 20 Oe are shown.

Table 1. Magnetization data obtained from the magnetization measurements for $HfFe_2$ sample. The saturation magnetization (M_s), the remanent magnetization (M_r), the coercive field (H_c) and the magnetic moment per unit formula ($\mu_{\rm UF}$) are reported. Uncertainties on the measured values are given in parentheses as errors on the last digit.

T[K]	M_s[emu/g]	M_r[emu/g]	H_c[Oe]	μ_{UF}/μ_B
5	60(1)	0.6(1)	7(1)	3.12(4)
298	55(1)	0.7(1)	8(1)	2.86(4)

The saturation magnetization (M_s) was evaluated by extrapolation of the magnetization versus $1/H$ for $H \to \infty$. The saturation magnetization value, obtained in this way, is 60 emu/g. The magnetization exceeds 90% of the saturation value in a field of 1000 Oe. The magnetic moment per formula unit for this sample was deduced from the saturation magnetization value at low temperature, and was found to be 3.12 μ_B. All the measured data are given in Table 1. As can be seen, $HfFe_2$ exhibits low values of remanent magnetization and coercitive field, which is typical for soft magnetic materials.

Figure 4 shows the Mössbauer absorption spectrum for the same sample at room temperature. The spectrum consists of two superimposed magnetic spectra, each of six

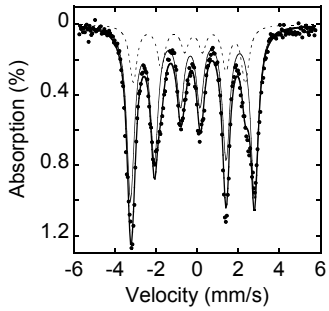

Fig. 4. Mossbauer absorption spectrum recorded at room temperature of the $HfFe_2$ sample; the experimental data (dots) and the fit curve (thick continuous line) are shown. The sextets associated with the component I (dashed line) and the component II (thin continuous line) are plotted.

Table 2. Mössbauer parameters obtained by fitting the absorption spectrum of $HfFe_2$ the table shows the values of isomer shift (δ), full width at half maximum of the absorption peaks (Γ), quadrupole splitting ($\Delta = eQV_{zz}/2$), hyperfine internal magnetic field (B_{hf}) and area of each component. Uncertainties on the measured values are given in parentheses as errors on the last digit.

Component	δ	Γ	Δ	B_{hf}	Area
	[mm/s]	[mm/s]	[mm/s]	[T]	[%]
I	–0.18(1)	0.44(1)	–0.21(1)	17.0(1)	25
II	–0.18(1)	0.44(1)	0.11(1)	18.9(1)	75

resonances, with a relative intensity ratio of 1 : 3, which are attributed to the two crystalographically inequivalent iron sites, 2a and 6h, in the C14 structure. The results of the least squares fits are summarized in Table 2; the values of the isomer shift, quadrupole splitting ($\Delta = eQV_{zz}/2$) and hyperfine magnetic field are reported. The values marked as I and II refer to the components in the spectra; the ratio of the area of the components has been fixed to 1 : 3 and the isomer shifts are forced to be equal on a basis of structural considerations [1].

4 Details of calculation

Electronic structure and hyperfine magnetic field calculations for both the hexagonal and cubic modification of $HfFe_2$, were performed using the full-potential augmented plane wave (FP-LAPW) method, based on density functional theory, as implemented in the WIEN 97 program package [11]. The LAPW method has proven to be well suited for calculating electronic properties in the solid state for periodic systems. In this method the unit cell is divided into non overlapping muffin-tin spheres around atoms and an interstitial region. In the spheres wave functions, charge density, and potential are expanded in spherical harmonics, while in the interstitial region they are expanded in plane waves. Additionally, the basis set is improved with local orbitals, in order to obtain better description of the low-lying semicore states. The muffin-tin radii for Hf and Fe were 2.3 and 2.15 a.u., respectively. The Brillouin zone integrations within the self-consistency cycles were performed via a tetrahedron method [12] using 195 and 76 k points in the irreducible wedge of the Brillouin zone for the C15 and C14 structure, respectively. The cut-off parameter $R_{MT}K_{max}$ for limiting the number of the plane waves was set to 8.5, where R_{MT} is the smallest value of all atomic sphere radii and K_{max} is the largest reciprocal lattice vector used in the plane wave expansion. The maximum l value for the waves used inside the atomic spheres was set to $l_{max} = 10$, whereas the charge density was Fourier expanded up to $G_{max} = 14$. The exchange and correlation effects were included within the generalized gradient approximation (GGA), using the parametrization given by Perdew-Burke-Ernzerhof [13]. The core-valence states separation was settled at –7 Ry. The core states were treated fully relativistically, while the valence states were treated within the scalar relativistic approximation. The spin-orbit contribution was neglected. For description of d states above the Fermi level, extra local orbitals were used in both cases. In our spin-polarized calculations, the self-consistency was achieved by demanding the convergence of the integrated charge difference between last two iterations to be smaller than 10^{-5} electron, since it ensures better stability of the calculated values than the corresponding energy criterion. For scalar-relativistic wave functions, the spin density at the nucleus, necessary for the computation of the hyperfine fields was computed averaging over a small region near the nucleus [14]. For the C15 structure volume optimization, changing the volume within ±5% of the experimental one and calculating the total energy as its function, was done. For the C14 structure, in addition to the volume and c/a optimization, it was necessary to relax the internal parameters. As the first step of structural relaxation, the atomic positions were relaxed according to Hellmann-Feynman forces calculated at the end of each self-consistent cycle. The force minimization criterion was 1.5 mRy/a.u. During this relaxation the cell volume and the c/a value were fixed to their experimental values. Then the theoretical equilibrium volume was determined by fixing the atomic positions to their optimized values and further keeping the c/a ratio fixed. A series of calculations was carried out, changing the volume within ±5% of its experimental value and calculating the total energy as its function. In the last step the c/a ratio was optimized by changing it within ±2% of the experimental value while keeping the optimized volume fixed. The results of these optimizations are shown in Figures 5 and 6.

5 Calculation results

The theoretically determined cell and structure parameters for the two structures, along with the experimental values obtained from X-ray diffraction measurements are given in Table 3. In both cases the theoretical volume underestimates the experimental one by ∼2%. The bulk moduli B_0 obtained by fitting the data to the Murnaghan's equation of state [15] are 176.4 GPa and 166.1 GPa for the C15 and C14 structure, respectively.

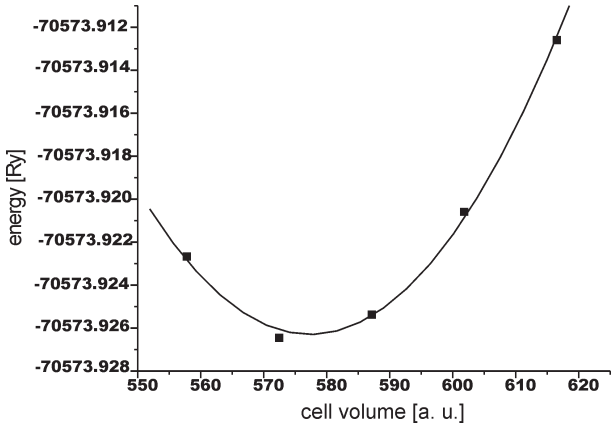

Fig. 5. Total energy vs. cell volume for the C15 $HfFe_2$ structure.

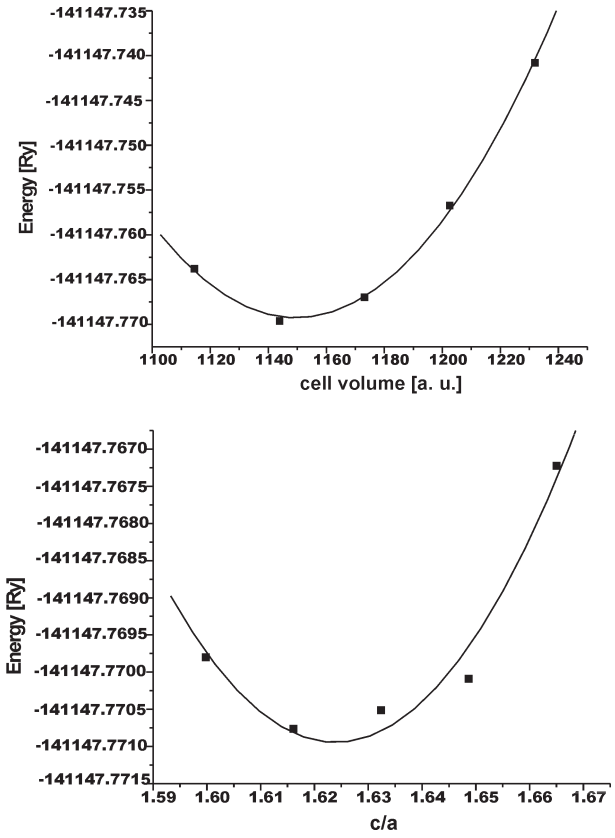

Fig. 6. Total energy vs. cell volume (top) and vs. c/a ratio (bottom) for the C14 $HfFe_2$ structure.

Table 4 reveals the site projected partial charge inside the muffin-tin (MT) spheres around Hf and Fe. The construction of the MT spheres is not unique and the charge contained within by no means corresponds to the actual ionic charge. Also, the charge in the interstitial region can not be assigned to any particular atomic species. Still, analyzing the charge confined in the MT spheres can be useful to get an overall picture about possible charge transfer between constituent atoms. From Table 4 it can be seen that there exists a spin-polarization of all states. It can also be observed that the s charge of Hf and Fe, as well as the d charge of Hf is redistributed, filling mostly the Fe p states and the interstitial region. This charge transfer is an indication that the bonds in this metallic compound could also have partly ionic character. Interstitial charges for spin up and spin down differ for about 0.67 which points out that there is itinerant magnetism in this compound. Table 5 reveals the site projected partial charge inside the muffin-tin (MT) spheres around Hf and two Fe atoms in the C14 $HfFe_2$ structure. It can be seen that there is no significant difference compared to the results obtained for the C15 structure. Both structures are very similar localy which can be seen from the composition and interatomic distances of the first coordination shell around all constituent atoms. The first coordination shell around Hf atom in the C15 structure consists of 12 Fe atoms at 2.898 Å and 4 Hf atoms at 3.027 Å, whereas in the C14 structure it breaks into six Fe subshells with distances in the interval from 2.878 to 2.898 Å and three Hf subshells with distances in the interval from 3.021 to 3.024 Å. The first coordination shell around Fe atom in the C15 structure consists of 6 Fe atoms at 2.471 Å and 6 Hf atoms at 2.898 Å, while in the C14 structure the distances around Fe 6h are almost identical. This is also true for the Fe 2a position. This explains why the calculated values for the partial charges within the MT spheres around the corresponding atoms in both structures are so similar.

Table 3. The parameters of the C15 and C14 $HfFe_2$ structure. The distances are in Å.

	Experimental results (X-ray diffraction)	WIEN 97
C15		
a	7.034 (2)	6.990
C14		
u	0.065	0.062
v	0.824	0.832
a	4.974 (1)	4.946
c	8.114 (3)	8.032

In Table 6, the calculated results for the magnetic moments and hyperfine magnetic fields are presented, for both atoms in the C15 $HfFe_2$ structure. The main contribution to the magnetic moments comes from the spin polarization of d states. As can be seen, the total magnetic moments for Hf and Fe have opposite direction and different intensity. Hf has small magnetic moment, implying that it is most likely generated by the Hf crystal environment. On the other hand, the iron magnetic moment is close to the value in elementar Fe, so it is obvious that the magnetic order in $HfFe_2$ originates completely from the Fe atomic magnetism. The hyperfine fields B_{hf} are composed of contributions from the core B_c and that from the valence electrons B_v. In the case of Hf atom, B_v is dominant, originating from the spin polarization of the valence electrons due to the magnetic moment on the Fe atom. For the Fe atom, B_c is dominant although B_v is significant too.

Table 4. l-decomposed site-projected charge inside the muffin-tin spheres around Hf and Fe in the C15 $HfFe_2$ structure.

Spin	Hf				Fe				interstitial
	s	p	d	f	s	p	d	f	
Up	1.090	2.939	0.442	6.974	1.170	3.139	3.895	0.007	5.486
Down	1.097	2.968	0.670	6.973	1.165	3.151	1.975	0.007	6.153
Total	2.187	5.907	1.112	13.947	2.335	6.290	5.870	0.014	11.639

Table 5. l-decomposed site-projected charge inside the muffin-tin spheres around Hf and two inequivalent Fe atoms in the C14 $HfFe_2$ structure.

Spin		up	down	total
Hf	s	1.088	1.098	2.186
	p	2.940	2.969	5.909
	d	0.440	0.675	1.115
	f	6.974	6.973	13.947
Fe 2a	s	1.169	1.165	2.334
	p	3.129	3.156	6.285
	d	3.872	2.010	5.882
	f	0.007	0.006	0.013
Fe 6h	s	1.169	1.166	2.335
	p	3.136	3.154	6.290
	d	3.873	2.005	5.878
	f	0.007	0.007	0.014
Interstitial charge		10.870	12.345	23.215

Table 6. The calculated hyperfine magnetic fields in the C15 $HfFe_2$ structure.

Atom	Contribution				Total magnetic moment	B_v[T]	B_c[T]	B_{hf}[T]
	s	p	d	f				
Hf	– 0.007	– 0.029	– 0.228	0.001	0.263	19.20	0.75	19.94
Fe	0.005	– 0.012	1.92	0	1.913	– 33.28	49.97	16.69

The calculated results for the magnetic moments and hyperfine magnetic fields, for all three atoms in the C14 structure are shown in Table 7. The difference in the calculated hyperfine magnetic fields at the two non-equivalent Fe positions is mainly due to the difference in the valence contributions. The calculated field at Hf position in the C14 structure is almost two times larger than the corresponding one in the C15 structure. Although this result may be suprising, it is very well known that the hyperfine interaction parameters are very sensitive to small changes of the interatomic distances and fine details of the electronic structure.

This difference in the hyperfine magnetic field values at Hf position in the two structures originates from the change of the valence contribution, while the core contributions in the two structures are almost identical. Considering the fact that the spin-orbit contribution is neglected in the calculations, the main contribution to the calculated hyperfine magnetic fields comes from the Fermi contact term, which originates from the spin polarization of the valence and core s states. It turns out that the increase of valence contribution to the hyperfine magnetic field at Hf position is a consequence of the increase of the spin polarization of the valence states with the significant charge density in the vicinity of the nucleus, i.e. s states. It is interesting to notice that the ratio of the calculated spin magnetic moments of the valence s electrons for the two structures, is 1.43 which is similar to the ratio of the calculated hyperfine magnetic fields at Hf positions in the two structures. The calculated magnetic moment per formula unit (3.06 μ_B) is in good agreement with the measured value of 3.12 μ_B.

6 Comparison with experiment and discussion

The HMF at Fe sites in the C14 $HfFe_2$ structure were investigated by Xia et al. [10], and their obtained values are in excellent agreement with both our measured and calculated values. The corresponding HMF in the C15 $HfFe_2$ structure were investigated by Livi et al. [3]. Their measurement using Mossbauer spectroscopy revealed two different values for hyperfine magnetic field at Fe site in this structure, which are attributed to the two crystalographically equivalent, but magnetically inequivalent Fe sites [16]. Although we cannot distinguish in our calculations the two magnetically inequivalent Fe sites in C15 structure, the agreement between the calculated and weighted mean measured value is fair.

The hyperfine magnetic fields at Hf site in $HfFe_2$ were investigated by three experimental groups [3,9,17], by employing the time differential perturbed angular correlation (TDPAC) method. Because of the nature of the method involved (the measurement actually takes place on the ^{181}Ta daughter isotope instead on the ^{181}Hf nucleus) it is not possible to make a direct comparison with the measured values. Still from Table 8 it can be seen that the obtained calculated value for HMF at Hf site in the C15 structure is not far away from the measured ones, especially having in mind the fact that the calculations by default are done at zero temperature and that the extrapolation of experimental results gives 18 T for HMF at Hf sites at 0 K [17]. This is not the case for the corresponding calculated value in the C14 $HfFe_2$ structure. This value differs substantially from the measured ones indicating that in this case it is necessary to make calculations with the Ta impurity involved.

In Table 8 all the reported experimental results for HMF in $HfFe_2$ (given in units of tesla), along with the calculated ones are given for clearness. Taking all the mentioned facts into account, we can conclude that generally the LAPW method is capable to calculate HMFs in metals precisely.

Table 7. The calculated hyperfine magnetic fileds in the C14 $HfFe_2$ structure.

Atom	Contribution				Total magnetic moment [μ_B]	B_{val}[T]	B_{cor}[T]	B_{hf}[T]
	s	p	d	f				
Hf	–0.01	– 0.029	– 0.235	0.001	0.264	30.94	0.81	31.75
Fe 2a	0.004	– 0.027	1.862	0.001	1.84	–32.25	48.34	16.08
Fe 6h	0.003	– 0.018	1.868	0	1.853	–29.73	48.66	18.93

Table 8. Comparison between the calculated and measured HMF values in $HfFe_2$. The values are in T. All measured values are refered to room temperature, except in reference [17] where the temperature is 78 K.

	Livi et al. [3]	Akselrod et al. [9]	Belosevic-Cavor et al. [17]	Xia et al. [10]	Our measurements	WIEN 97
C15						
Hf	13.0(4)	14.2(4)	15.95(9)			19.9
Fe	17.6(4)					16.7
	18.4(4)					
C14						
Hf	8.5(5)	14.6(4)				31.8
Fe 2a				16.9	17.0(1)	16.1
Fe 6h				18.8	18.9(1)	18.9

7 Summary

In summary, we have presented recent results of experimental and theoretical studies of hyperfine magnetic fields in $HfFe_2$ and provided further insights into the electronic and magnetic properties of this intermetallic compound. We have measured the saturation and the remanent magnetization, the coercive field, the magnetic moment per formula unit and the hyperfine magnetic field at Fe site in the C14 $HfFe_2$ structure. We have also calculated the structure parameters, magnetic moments, partial charges and hyperfine magnetic fields in both possible $HfFe_2$ structures, C15 and C14. Our calculations show that localy these structures are very similar. On the other hand, the hyperfine interaction parameters are very sensitive to fine details of the electronic structure and consequently the hyperfine magnetic field differ considerably, especially at Hf position. The excellent agreement between the calculated and measured magnetic moment per formula unit is a good indication of the quality of our calculations.

This work has been partly supported by the grant No. 141 022 G from the Serbian Ministry of Science and Environmental Protection.

References

1. K. Ikeda, Z. Metallkde **68**, 195 (1977)
2. K. Terao, M. Shimizu, Phys. Stat. Sol. (b) **139**, 485 (1987)
3. F.P. Livi, J.D. Rogers, P.J. Viccaro, Phys. Stat. Sol. (a) **37**, 133 (1976)
4. A.M. van der Kraan, P.C.M. Gubbens, K.H.J. Buschow, J. Phys. **41**, 1, C1-189 (1980)
5. T. Nakamichi, K. Kai, Y. Aoki, K. Ikeda, M. Yamamoto, J. Phys. Soc. Jpn **29**, 794 (1970)
6. K. Kai, T. Nakamichi, J. Phys. Soc. Jpn **30**, 1755 (1971)
7. M. Shiga, Y. Muraoka, Y. Nakamura, J. Magn. Magn. Mater. **10**, 280 (1979)
8. F.P. Livi, Sol. Stat. Comm. **22**, 107 (1977)
9. Z.Z. Akselrod, M. Budzynski, P. Khazatrov, B.A. Komissarova, L.N. Kryukova, S.I. Reiman, G.K. Ryasny, A.A. Sorokin, Hyperfine Interactions **14**, 7 (1983)
10. S.K. Xia, H. Saitovich, P.R.J. Silva, J.A. Gomez, F.C. Rizzo Assuncao, E. Baggio-Saitovich, J. Phys. Condens. Matt. **10**, 345 (1998)
11. P. Blaha, K. Schwarz, J. Luitz, WIEN 97 (Vienna University of Technology, Vienna 1977). Improved and updated UNIX version of the original copyrighted WIEN code, which was published by P. Blaha, K. Schwarz, P. Sorantin, S.B. Trickey, Comput. Phys. Commun. **59**, 399 (1990)
12. P.E. Blochl, O. Jepsen, O.K. Andersen, Phys. Rev. B **49**, 16223 (1994)
13. J.P. Perdew, S. Burke, M. Ernzerhof, Phys. Rev. Lett. **77**, 3865 (1996)
14. S. Blügel, H. Akai, R. Zeller, P.H. Dederichs, Phys. Rev. B **35**, 3271 (1987)
15. F.D. Murnaghan, Proc. Natl. Acad. Sci. U.S.A. **30**, 244 (1944)
16. G.K. Wertheim, V. Jaccarino, J.H. Wernick, Phys. Rev. **135**, 1A, A151 (1964)
17. J. Belošević-Cavor, N. Novakovic, B. Cekic, N. Ivanovic, M. Manasijevic, J. Magn. Magn. Mater. **272–276**, 762 (2004)